(Preprint) AAS 17-374

A NEW MULTI-TARGET TRACKING ALGORITHM FOR A LARGE NUMBER OF ORBITING OBJECTS

E. D. Delande [*], J. Houssineau [†], J. Franco [‡], C. Frueh [§], D. E. Clark [¶]

This paper demonstrates the applicability of the filter for Hypothesised and Independent Stochastic Populations (HISP), a multi-target joint detection/tracking algorithm derived from a recent estimation framework for stochastic populations, to wide area surveillance scenarios in the context of Space Situational Awareness. Designed for multi-object estimation problems where the data association between targets and collected observations is moderately ambiguous, the HISP filter has a linear complexity with the number of maintained tracks and the number of observations, and is a scalable filtering solution adapted to large-scale target tracking scenarios. It is illustrated on a challenging surveillance problem involving 30 targets on different orbits, observed by 3 sensors with limited coverage, measurement noise, false alarms, and missed detections.

INTRODUCTION

In the context of Space Situational Awareness (SSA), the representation of an identified orbiting object within a catalogue typically relies on its Two-Line Elements (TLEs), providing information on the current object's dynamical components (position, velocity) in the near-Earth space. While objects known through a significant number of past observations collected from sensing assets can be represented by a highly accurate orbit, no measure of the *uncertainty* associated to this information is maintained through the TLEs, even though the process of collecting information on orbiting objects is affected by many sources of error (orbital motion model, sensors' noise characteristics, false alarms, missed detections, data association between objects and collected measurements, etc.). The TLEs are ill-adapted to the representation of objects for which little *a priori* information is available – for example, in the initial orbit determination procedure for a piece of debris or unknown object observed for the first time – and, more generally, space-related tasks crucial to the safety of the space environment would benefit from a systematic and principled exploitation of the catalogue beyond the extraction of point estimates for individual objects.

A natural approach to address this issue is to cast the orbital tracking problem within a Bayesian estimation framework, because a probabilistic description of an object's state allows for the representation of uncertainty in the propagated information. For this reason, there has been a growing interest in the design of target detection/tracking Bayesian algorithms adapted to the specifics of the SSA surveillance activity. This task presents two main challenges:

1. On the single-object level, observations collected by sensing assets are reasonably accurate, but they are incomplete (for example, radio-frequency sensors lack information on the object's angle velocities). Observations of space assets are unusually scarce for a detection/tracking problem, as most objects are only visible through a short window of time by a given sensor. On the other hand, the dynamics of objects are better known than in most tracking applications, since orbital motion models are understood and numerically calculable to a reasonable degree of accuracy.

[*] Research Associate, Heriot Watt University, School of Engineering & Physical Sciences, Edinburgh, UK, E.D.Delande@hw.ac.uk
[†] Visiting Researcher at CSIRO Data61, Eveleigh, Australia, houssineau.j@gmail.com
[‡] PhD student, Heriot Watt University, School of Engineering & Physical Sciences, Edinburgh, UK, jf139@hw.ac.uk
[§] Assistant Professor, Purdue University, School of Aeronautics & Astronautics, West Lafayette, U.S.A., AIAA member, cfrueh@purdue.edu
[¶] Associate Professor, Heriot Watt University, School of Engineering & Physical Sciences, Edinburgh, UK, D.E.Clark@hw.ac.uk

2. On the multi-object level, the number of orbiting objects is unknown and time-varying, and needs to be estimated alongside their state. The data association between objects in the catalogue and collected observations is unknown and needs to be estimated as well, though it is less ambiguous than in most tracking applications where objects are closer from each other with respect to (w.r.t.) to the sensor resolution. Missed detections and false positives, though perhaps less frequent than in other tracking applications, occur nonetheless. The growing number of objects to be detected, identified, and tracked, whether man-made satellites or space debris,[1] presents a specific challenge to any multi-object filtering architecture.

Historical developments in multi-target tracking focused on the design on applications for radars in a military context.[2,3] The track-based solutions, such as the Multiple Hypothesis Tracking (MHT) filter,[4] are designed as an extension of the single-target tracking problem to the multiple target case. The construction of tracks from a sequence of coherent observations follows an intuitive approach, and the creation/deletion of tracks typically rely on heuristics based on expert knowledge adapted to the specifics of the surveillance scenario. An example of a track-based solution applied to SSA can be found in.[5] Track-based approaches typically rely on an explicit construction of the data association between tracks and observations and, consequently, are costly to maintain in terms of memory space and computational power. This is perhaps the main reason for the initial popularity of set-based approaches in the late 1990s and early 2000s,[6,7] and their steady development ever since. Set-based methods approach the multi-object estimation problem in a holistic manner and incorporate all the sources of uncertainty (appearance/disappearance of targets, observation process, etc.) in a unified probabilistic framework. While the most general set-based Bayesian filter is intractable, the Finite Set Statistics methodology[8] provides principled derivation tools to produce approximate solutions propagating a reduced but tractable amount of information. The original set-based solutions, such as the Probability Hypothesis Density (PHD) filter,[7] avoid any explicit data association and can potentially handle scenarios with large number of targets. This is done, however, at the expense of track continuity, as these filters do not maintain individual information on specific targets (e.g. tracks) but only a collective representation of the targets as a single population of objects. With the increased capabilities of computers, the development of set-based solutions maintaining track custody of individual targets has enjoyed significant popularity in the recent years.[9] Applications of set-based solutions to the SSA context can be found in.[10–16]

A recent estimation framework for stochastic populations,[17] applied to multi-target estimation problems, proposes an alternative unified probabilistic description and introduces the notion of target distinguishability, allowing for the representation of a target either as an unidentified member of larger population or as an individual track, depending on the information collected so far. The filter for Distinguishable and Independent Stochastic Populations (DISP)[18] was used on a multi-target SSA scenario where the number of objects and their states are jointly estimated from the collected observations.[19,20] The DISP filter was designed for challenging scenarios where the data association is highly ambiguous – typically, when targets have crossing trajectories or evolve close to each other for long periods of time – and its computational cost grows significantly with the number of targets involved in the surveillance scenario.

Expanding from the promising results obtained with the DISP filter in the SSA context, this paper explores further the approach presented in[19,20] through the following points:

1. The multi-object filtering architecture exploits the filter for Hypothesised and Independent Stochastic Populations (HISP), a principled approximation of the DISP filter designed for scenarios where the data association is moderately ambiguous.[17,21] The HISP filter is far less computationally expensive than the DISP filter whilst still maintaining track custody on detected objects, and will allow to scale the SSA problem from a few objects to potentially hundreds of them.
2. The single-target Bayesian time update step in[19,20] exploited a Cartesian coordinate system and the orbiting objects were propagated through the Shepperd matrix;[22,23] in this paper the target space will be constructed with a set of orbital elements,[24] allowing for a more natural construction of the process noise in the prediction model.

THE ESTIMATION FRAMEWORK FOR STOCHASTIC POPULATIONS

This section provides a broad description of the context in which the HISP filter was developed. More detailed information on the estimation framework for stochastic populations can be found in.[17] The HISP filter is covered in more detail in.[21,25] The DISP filter, a more general solution from which the HISP filter is derived as a principled approximation, is explained in detail in.[18] The former filter has been exploited in the context of SSA in.[19,20]

This estimation framework proposes a unified probabilistic description of all the sources of uncertainty in a generic multi-sensor multi-object detection and tracking problem (sensors' characteristics, object dynamical behaviour, number of objects, etc.). The filtering solutions derived from this framework, such as the DISP and the HISP filters, follow a principled construction and rely on a set of well-defined assumptions; different assumptions lead to algorithms with different complexity, which are adapted to particular scenarios. This framework proposes a probabilistic representation of the population of interest through two levels of uncertainty:

1. On the individual level, the targets of the population of interest are represented by *tracks*. Each track describes the current state (e.g. orbital elements) of the target(s) associated to it*. A track does not necessarily represent a *single* target; it can represent *collectively* a sub-population of targets who are *indistinguishable* from one another for the purpose of estimation. The concept of target indistinguishability is a key element of this estimation framework and will be discussed in more details later on in the paper.
2. On the population level, the composition of the population of interest is represented by *multi-target configurations*. Each multi-target configuration proposes a combination of tracks with associated *multiplicity* – the number of targets represented by each track – as a representation of the total population of interest. A multi-target configuration is associated to a scalar *weight*, describing the probability that this configuration reflects the true composition of the population of interest.

Bayesian filtering

The considered estimation framework, when applied to multi-target detection and tracking problems, is set within the Bayesian paradigm, i.e., a sequence of *time prediction* and *data update* steps in which the information on the population of interest is propagated through time using the operator's knowledge and corrected through the observation collected from a sensor, respectively.

Without loss of generality, the time is indexed by the set $\mathbb{T} \doteq \mathbb{N}$. For any $t \in \mathbb{T}$, the target state space of interest $\mathbf{X}_t^\bullet \subseteq \mathbb{R}^d$ describes the physical characteristics of interest for a target (e.g., position and velocity components in Cartesian coordinates, or a set of orbital elements), and the observation space of interest $\mathbf{Z}_t^\bullet \subseteq \mathbb{R}^{d'}$ describes the measurable quantities collected from one observation (e.g. range, azimuth, elevation, and range rate for a radar with Doppler effect). They are augmented with the *empty state* ψ and the *empty observation* ϕ, respectively, to form the *(full) target state space* $\mathbf{X}_t = \mathbf{X}_t^\bullet \cup \{\psi\}$ and the *(full) observation space* $\mathbf{Z}_t = \mathbf{Z}_t^\bullet \cup \{\phi\}$. The empty state ψ describes the state of targets outside of the scene of interest (e.g., an object that disintegrates in the atmosphere of Earth). The empty observation ϕ describes missed detections, i.e., when an object fails to produce a detection.

Note that in the context of this paper, the target state space $\mathbf{X}_t$ is constant across the scenario since the scene of interest consists in a fixed volume of space around Earth; the observation state space $\mathbf{Z}_t$, however, can vary since different sensors can be exploited sequentially across the scenario. At each time $t \in \mathbb{T}$, the sensor is assumed to be a finite-resolution sensor whose resolution cells (e.g. pixels, radar cells) are indexed by Z_t'; a set of observations $Z_t \subseteq Z_t'$ corresponding to cells where a signal has been detected is made available. The set of collected observations is denoted $\bar{Z}_t$ when augmented with the empty observation ϕ.

*Past states are also available through the track history.

Individual level: tracks and observation paths

Each track represents a sub-population of targets *indistinguishable* from each other, because the same information is known on each of them. The probability density p on $\mathbf{X}_t$ associated to a track describes the state of *each* individual of the sub-population of targets it represents*. In the context of SSA as in many tracking applications, the most direct way to distinguish targets is to consider their observation histories. For this reason, we consider the space $\bar{\mathbb{O}}_t$, defined as the Cartesian product

$$\bar{\mathbb{O}}_t \doteq \bar{Z}_0 \times \cdots \times \bar{Z}_t, \tag{1}$$

so that $\boldsymbol{o}_t \in \bar{\mathbb{O}}_t$ takes the form $\boldsymbol{o}_t = (\phi, \ldots, \phi, z_{t_+}, \ldots, z_{t_-}, \phi, \ldots, \phi)$ with t_+ and t_- the time of appearance and disappearance of the considered track in the scene of interest, and with $z_t \in \bar{Z}_t$ for any $t_+ \leq t \leq t_-$. The observation history $\boldsymbol{o}_t$ can also be referred to as the *observation path* and the empty observation path $(\phi, \ldots, \phi) \in \bar{\mathbb{O}}_t$ is denoted $\boldsymbol{\phi}_t$. Note that a target cannot produce an observation while outside of the scene of interest, i.e., before its time of appearance or after its time of disappearance.

Each target is identified by some index $\boldsymbol{i}$ in a set $\mathbb{I}$, whose nature depends on the filter (detailed later on for the HISP filter). The DISP and HISP filters both rely on the modelling assumptions that, at any time $t \in \mathbb{T}$:

M.1 A target produces at most one observation (if not, a *missed detection* occurs),
M.2 An observation originates from at most one target (if not, a *false positive* or *false alarm* occurs).

An important consequence of **M**.1, **M**.2 is that an observation characterises an *individual* target. A track $\boldsymbol{i}$ associated to an observation path with a least one detection (i.e., $\boldsymbol{o}_t^{\boldsymbol{i}} \neq \boldsymbol{\phi}_t$) cannot have a multiplicity $n^{\boldsymbol{i}}$ greater than one since it cannot represent more than one target. The *previously-detected* target represented by the track $\boldsymbol{i}$ is then *distinguishable*, and the probability density $p^{\boldsymbol{i}}$ describes the state of *that individual and no one else*. On the contrary, a track $\boldsymbol{i}$ associated to the empty observation path $\boldsymbol{o}_t^{\boldsymbol{i}} = \boldsymbol{\phi}_t$ represents a sub-population of *yet-to-be-detected* targets that are indistinguishable from one another, and may have a multiplicity $n^{\boldsymbol{i}}$ greater than one.

Population level: multi-target configurations

The probabilistic description of the composition of the population is maintained through multi-target configurations, associating a multiplicity to each track to describe a specific composition. In particular, a track $\boldsymbol{i}$ with multiplicity $n^{\boldsymbol{i}} = 0$ in a given multi-target configuration does not exist according to that configuration, i.e. the sub-population of targets it represents are not physical objects of the population of interest. Both the DISP and the HISP filters rely on the modelling assumptions that

M.3 Target evolve independently from each other,
M.4 Observations resulting from target detections are produced independently from each other.

The modelling assumptions mentioned so far allow for a rich representation of the population, with the tracks covering all the possible combinations of non-empty observation paths representing the previously-detected targets (see Figure 1), and one (or possibly several) track(s) representing sub-population(s) of yet-to-be-detected targets. In many tracking applications, the prior information on appearing objects is scarce and little is known on objects prior to their first detection. In that case, the information maintained on the various sub-populations of yet-to-be-detected targets is similar and little is gained from propagating them separately. The estimation framework for stochastic population provides principled tools for the *mixing* of such populations, and both the DISP† and the HISP filters rely on the simplifying assumption that, at any time $t \in \mathbb{T}$,

S.1 The appearing targets and the yet-to-be-detected targets are mixed in a single sub-population.

*For example, a unique track may describe *each* of the pieces of debris following a collision *before* some specific information is acquired on individual pieces through an observation.

†Several versions of the DISP filter are proposed in[18] depending on whether they rely on **S**.1, a tighter version, or a looser version of it.

An important consequence of **S**.1 is that the DISP and HISP filters maintain a *single* track $\mathrm{u} \in \mathbb{I}$ for *all* the yet-to-be-detected (or **u**ndetected) objects.

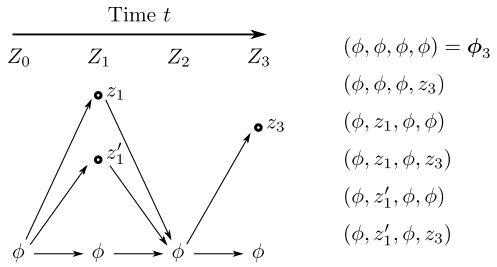

Figure 1: The observation paths at time $t = 3$, given a sequence of collected observations.

A general filtering solution: the DISP filter

Essentially, the DISP filter imposes no further restrictions on the system and relies on the modelling and simplifying assumptions described so far. A possible composition of the population of targets is given by:

1. A subset of pairwise compatible* tracks $H \subseteq \mathbb{I}_t \setminus \{\mathrm{u}\}$, representing the previously-detected targets,
2. The undetected track u, with multiplicity $n^{\mathrm{u}} \in \mathbb{N}$, representing a sub-population of n^{u} yet-to-be-detected targets.

Each subset of pairwise compatible tracks $H \subseteq \mathbb{I}_t \setminus \{\mathrm{u}\}$ is called an *hypothesis*, and the set of all the hypotheses is denoted by $\mathbf{H}_t$. The DISP filter maintains a full probabilistic representation of the composition through the set of all the multi-target configurations $(H, n^{\mathrm{u}}) \in \mathbf{H}_t \times \mathbb{N}$ with associated weights $\mathbf{w}_t(H, n^{\mathrm{u}}) \in \mathbb{R}^+$ such that

$$\sum_{(H,n^{\mathrm{u}}) \in \mathbf{H}_t \times \mathbb{N}} \mathbf{w}_t(H, n^{\mathrm{u}}) = 1. \tag{2}$$

Note that the probabilities of existence $w_t^{\boldsymbol{i}}$ of the previously-detected tracks $\boldsymbol{i} \in \mathbb{I}_t \setminus \{\mathrm{u}\}$ and the cardinality distribution $\{\rho_t^{\mathrm{u}}(n)\}_{n \in \mathbb{N}}$ of the sub-population of yet-to-be-detected targets can be defined via the marginalizations

$$w_t^{\boldsymbol{i}} = \sum_{\substack{(H,n^{\mathrm{u}}) \in \mathbf{H}_t \times \mathbb{N} \\ H \ni \boldsymbol{i}}} \mathbf{w}_t(H, n^{\mathrm{u}}), \;\; \boldsymbol{i} \in \mathbb{I}_t \setminus \{\mathrm{u}\} \qquad \text{and} \qquad \rho_t^{\mathrm{u}}(n) = \sum_{H \in \mathbf{H}_t} \mathbf{w}_t(H, n), \;\; n \in \mathbb{N}. \tag{3}$$

The DISP filter was specifically designed for challenging scenarios where the data association between targets and observations can be highly ambiguous since, similarly to the MHT filter, it maintains the joint existence of any subset of tracks based on their full observation paths. Even though it can be exploited on a SSA scenario with a small number of targets,[19,20] its computational complexity grows dramatically with the number of observations and/or targets, making this solution ill-adapted to large-scale tracking scenarios.

Alleviating the computational complexity of the DISP filter: the HISP filter

The HISP filter is a principled approximation of the DISP filter that aims to provide a scalable filtering solution adapted to scenarios involving a large number of objects. It is based on the assumption that any two tracks are unlikely to have generated the same observation in Z_t. In other words, the origin target of an observation is assumed moderately ambiguous, which fits the context of SSA where the orbiting objects evolve reasonably far away from each other w.r.t. the resolution of the typical sensors. As it will be seen later, this assumption simplifies dramatically the data update step of the DISP filter to a structure with linear complexity w.r.t. the number of hypotheses and observations.

*Recall from the modelling assumption **M**.2 that an observation originates from at most one object, and thus two distinct tracks whose observation paths share a non-empty observation cannot exist simultaneously.

THE HISP FILTER

Integration and likelihood in the HISP filter

Since the state space $\mathbf{X}_t$ at time $t \in \mathbb{T}$ is made of a continuous part ($\mathbf{X}_t^\bullet$) and of a discrete part (ψ), probability densities and transitions have to be introduced in a specific way: they are defined w.r.t. the Lebesgue measure on $\mathbf{X}_t^\bullet$ and by the probability mass on ψ. Similarly, the integral of a function f on $\mathbf{X}_t$ is defined as

$$\int f(x)\mathrm{d}x = \int_{\mathbf{X}_t^\bullet} f(x)\mathrm{d}x + f(\psi). \tag{4}$$

The observation space is also made of a continuous and a discrete part, which requires the use of a specific observation update as follows. Let p be a probability density function and l_z an integrable function defined on the same space $\mathbf{X}_t$, and consider the formula

$$\hat{p}(x) = \frac{l_z(x)p(x)}{\int l_z(x')p(x')\mathrm{d}x'}, \tag{5}$$

defined whenever $\int l_z(x')p(x')\mathrm{d}x' > 0$. The function l_z in (5) is referred to as a *potential* since it reshapes p by increasing or discarding the probability given by p depending on the values taken by l_z. If l_z is interpreted as the probability density function corresponding to some likelihood on $\mathbf{X}_t$ evaluated at the observation $z \in \mathbf{Z}_t^\bullet$, then $\hat{p}$ is the Bayes' posterior measure given z corresponding to the prior p. Moreover, if p is Gaussian and the observation process is linear and Gaussian, then $\hat{p}$ is the Kalman filter posterior distribution. Solutions to the multi-target tracking problem in the linear Gaussian case can be formulated in terms of Kalman filters in interaction[26,27] and depend on the value of the denominator in Bayes' theorem. In the one-dimensional observation case, this denominator would be of the form

$$\int l_z(x)p(x)\mathrm{d}x = \frac{1}{\sqrt{2\pi}\varsigma}\exp\left(-\frac{(Hm-z)^2}{2\varsigma^2}\right), \tag{6}$$

where H is the observation matrix, where $\varsigma^2 = HVH^{\mathrm{T}} + \sigma^2$ with σ the variance of the observation noise, where m and V are the mean of variance of the prior distribution and where $\cdot^{\mathrm{T}}$ is the matrix transposition. Note that this quantity depends on the reference measure considered for defining the density $(x, z) \mapsto l_z(x)$. This remark has little relevance in the context of single-object tracking, since a change of scale in the density l_z affects the numerator and denominator of (5) in the same way; it is, however, problematic in the multi-object case as the denominator (6) can be used to assess data association events and compare them to other events that are not affected by the change of scale.

Suppose, for example, that the observation state space represents position coordinates in some Cartesian frame, and that the reference measure is modified so that distances are now measured in *metres* rather than *kilometres*. It makes any volume in the observation space *larger*, and thus the scalar (6) becomes *smaller* because of the term in the denominator of the right-hand side. The association between this observation and this target becomes less likely when compared to other events that have not been modified by this change in the reference measure - typically, the association of the same target with *no observation* (i.e., a missed detection event).

Making l_z an element of $\mathbf{L}(\mathbf{X}_t)$, the set of integrable functions on $\mathbf{X}_t$ with supremum equal to one, rather than a probability density alleviates this issue without affecting the result in the single target case because of the normalisation factor. The resulting potential is the Gaussian-shaped function defined, in the one-dimensional case, as

$$l_z(x) = \exp\left(-\frac{(Hx-z)^2}{2\sigma^2}\right). \tag{7}$$

With this approach, we find that

$$\int l_z(x)p(x)\mathrm{d}x = \frac{\sigma}{\varsigma}\exp\left(-\frac{(Hm-z)^2}{2\varsigma^2}\right), \tag{8}$$

which is dimensionless, takes value in the interval $[0, 1]$ and can be interpreted as the probability for the observation z to belong to the target with distribution p. Since l_z, as a function of z, is not defined as a density w.r.t. an arbitrary reference measure, it can be extended to $\mathbf{Z}_t$ in a natural way.

In practice, the observation process at time t is modelled by a potential ℓ_t^z on $\mathbf{X}_t$ defined for any $z \in \bar{Z}_t$ and verifying $\ell_t^\phi(\psi) = 1$, since targets that are not present in the scene cannot generate an observation. Typically, for any $x \in \mathbf{X}_t^\bullet$, the potentials ℓ_t^z can be rewritten as

$$\ell_t^z(x) = p_{\mathrm{d},t}(x) l_t^z(x), \;\; z \in Z_t \qquad \text{and} \qquad \ell_t^\phi(x) = 1 - p_{\mathrm{d},t}(x), \tag{9}$$

where $p_{\mathrm{d},t}$ is the *probability of detection* and the dimensionless potential l_t^z is the *likelihood of association* with measurement z – of the form (7) in the one-dimensional, linear Gaussian case.

Multi-target model and indexing of targets

Recall from the simplifying assumption **S**.1 that the appearing targets are mixed with the yet-to-be-detected targets, at each time $t \in \mathbb{T}$. Therefore, in the context of HISP filtering, the time of appearance in the scene of a target is unknown, and does not provide a way of identifying an individual of the population of interest. A target is then indexed by a pair $(t, \boldsymbol{o})$ where t is the last epoch where the target was known to be in the scene, and the observation path $\boldsymbol{o}$ stores its detections across time. More specifically, at any time $t \in \mathbb{T}$:

- an index $\boldsymbol{i} = (t', \boldsymbol{o})$, where $t' < t$, denotes a target that has already left the scene,
- an index $\boldsymbol{i} = (t, \boldsymbol{o})$ denotes a target that is still in the scene.

The HISP filter does not maintain a representation of the individuals of the former type for the purpose of filtering, but they can be exploited for the purpose of displaying (we will do so in the track extraction process later on). At any time $t \in \mathbb{T}$, then, the representations of the targets after the prediction and after the observation update can be indexed by the sets $\mathbb{I}_{t|t-1} = \{(t, \boldsymbol{o}) \,|\, \boldsymbol{o} \in \bar{\mathbb{O}}_{t-1}\}$ and $\mathbb{I}_t = \{(t, \boldsymbol{o}) \,|\, \boldsymbol{o} \in \bar{\mathbb{O}}_t\}$, respectively. It is useful to introduce additional symbols for representing some specific sub-populations: the targets with an index $(t, \boldsymbol{o}) \in \mathbb{I}_t$ that

(m) have been previously detected, or **m**easured, so that $\boldsymbol{o} \neq \boldsymbol{\phi}_t$ (the previously-detected targets),
(u) are in the state space but are **u**ndetected, so that $\boldsymbol{o} = \boldsymbol{\phi}_t$ (the yet-to-be-detected targets).

The single element in the set $\mathbb{I}_t^{\mathrm{u}}$ is denoted $\boldsymbol{i}_t^{\mathrm{u}}$. Using the concept and notations defined above, the HISP filter can be expressed via a set of *hypotheses*[*], e.g. after the observation update at time t by a set of triples of the form $\mathcal{P}_t = \{p_t^{\boldsymbol{i}}, w_t^{\boldsymbol{i}}, n_t^{\boldsymbol{i}}\}_{\boldsymbol{i} \in \mathbb{I}_t}$, where $p_t^{\boldsymbol{i}}$ is the probability density corresponding to the index $\boldsymbol{i} \in \mathbb{I}_t$, $w_t^{\boldsymbol{i}} \in [0, 1]$ is the weight (or credibility, or probability of existence) of the hypothesis and where $n_t^{\boldsymbol{i}}$ is the multiplicity of the hypothesis, i.e., the potential number of targets having this representation. Note that the credibility $w_t^{\boldsymbol{i}}$ of a hypothesis is different from the probability $p_t^{\boldsymbol{i}}(\psi)$ that the corresponding target is absent from the scene, i.e., outside of the space $\mathbf{X}_t^\bullet$.

Simplifying assumptions

Approximations are required in order to maintain a low computational cost for the HISP filter. The first one ensures that all the terms in the observation update can be computed with a linear complexity by making an assumption on the term

$$\breve{w}_t^{\boldsymbol{k},z} = w_{t|t-1}^{\boldsymbol{k}} \int \ell_t^z(x) p_{t|t-1}^{\boldsymbol{k}}(x) \mathrm{d}x \tag{10}$$

which corresponds to the association of the target with index $\boldsymbol{k} \in \mathbb{I}_{t|t-1}$ with the observation $z \in Z_t$. The second one ensures that all individual hypotheses can be included in a single population hypothesis by breaking the correlation

[*]Note that each hypothesis maintained by the HISP filter corresponds to a track and is described by its own probability of existence, while each hypothesis maintained by the DISP filter corresponds to a subset of compatible tracks and is described by their joint probability of existence. In the context of HISP filtering, the term "track" more usually refers to a confirmed hypothesis in the track extraction process (detailed later).

between the probability of existence of the different multi-target configurations that naturally arise after time prediction and observation update. Specifically, it is assumed that:

S.2 For any $\boldsymbol{k}, \boldsymbol{k}' \in \mathbb{I}_{t|t-1}$ such that $\boldsymbol{k} \neq \boldsymbol{k}'$ and any $z \in Z_t$, it holds that $\breve{w}_t^{\boldsymbol{k},z} \breve{w}_t^{\boldsymbol{k}',z} \approx 0$,
S.3 Hypotheses are independent of each other.

The simplifying assumption **S.2**, mentioned earlier in the paper, supposes that the data association is moderately ambiguous. The simplifying assumption **S.3** implies that the probabilistic representation of the DISP filter on the population level, maintained through the joint probability of existence of every subset of compatible tracks, is collapsed to the individual level where each track is maintained alongside its marginalized probability of existence.

Time prediction

Any considered transition q from $\mathbf{X}_{t-1}$ to $\mathbf{X}_t$ is assumed to verify $\int q(x', x)\mathrm{d}x \leq 1$ for any $x' \in \mathbf{X}_{t-1}$. If it holds that $\int q(x', x)\mathrm{d}x = 1$ for any $x' \in \mathbf{X}_{t-1}$ then q is called a Markov transition. The motion of a target from time $t-1$ to time t is modelled by a Markov transition q_t^π verifying for any $x' \in \mathbf{X}_{t-1}^\bullet$

$$q_t^\pi(\psi, \psi) = 1 \qquad \text{and} \qquad q_t^\pi(x', \psi) = 0, \tag{11}$$

these modelling choices being justified by the fact that the transition q_t^π models propagation in the scene only, and includes neither target appearance nor disappearance of the scene. Also, the function $p_t^\pi(x) = \int q_t^\pi(x, x')\mathrm{d}x'$ is the probability that a target at point x at time $t-1$ does not disappear. The disappearance of a target between time $t-1$ and time t is modelled separately by a transition q_t^ω verifying for any $x' \in \mathbf{X}_{t-1}^\bullet$

$$\int_{\mathbf{X}_t^\bullet} q_t^\omega(x', x)\mathrm{d}x = 0 \qquad \text{and} \qquad \int q_t^\omega(\psi, x)\mathrm{d}x = 0. \tag{12}$$

The transition q_t^ω and q_t^π are assumed to be complementary in the sense that $q_t^\omega(x, \psi) + p_t^\pi(x) = 1$, i.e. either the target does disappear or it does not (the scalar $1 - q_t^\omega(x, \psi)$ is sometimes called the *probability of survival* of target with state x). Additionally, there are n_t^α targets potentially appearing at time t, modelled by a probability density q_t^α on $\mathbf{X}_t$ and by a scalar weight w_t^α.

In this section, the symbol "u" will be used in place of the indices $\boldsymbol{i}_{t-1}^{\mathrm{u}}$ and $\boldsymbol{i}_{t|t-1}^{\mathrm{u}}$ when there is no possible ambiguity. The newborn targets as well as the undetected ones are represented together after time prediction by

$$p_{t|t-1}^{\mathrm{u}}(x) = \frac{n_{t-1}^{\mathrm{u}} \int q_t^\pi(x', x) p_{t-1}^{\mathrm{u}}(x')\mathrm{d}x' + n_t^\alpha p_t^\alpha(x)}{n_{t-1}^{\mathrm{u}} + n_t^\alpha} \tag{13a}$$

$$(w_{t|t-1}^{\mathrm{u}}, n_{t|t-1}^{\mathrm{u}}) = \left(\frac{n_{t-1}^{\mathrm{u}} w_{t-1}^{\mathrm{u}} + n_t^\alpha w_t^\alpha}{n_{t-1}^{\mathrm{u}} + n_t^\alpha}, n_{t-1}^{\mathrm{u}} + n_t^\alpha \right). \tag{13b}$$

The targets that have already been observed at least once in the past and which have prior indices in $\mathbb{I}_{t-1}$ of the form $\boldsymbol{k} = (t-1, \boldsymbol{o})$, with $\boldsymbol{o} \neq \boldsymbol{\phi}_{t-1}$, can either be propagated (kernel q_t^π) or disappear (kernel q_t^ω); they are characterised after time prediction by

$$p_{t|t-1}^{\boldsymbol{i}}(x) = \int q_t^\iota(x', x) p_{t-1}^{\boldsymbol{k}}(x')\mathrm{d}x' \tag{14a}$$

$$(w_{t|t-1}^{\boldsymbol{i}}, n_{t|t-1}^{\boldsymbol{i}}) = (w_{t|t-1}^{i}, 1), \tag{14b}$$

with $\iota \in \{\pi, \omega\}$ and with $\boldsymbol{i}$ equals to $(t, \boldsymbol{o})$ if $\iota = \pi$ – the target is still in the scene at epoch t – and $(t-1, \boldsymbol{o})$ otherwise – the target has left the scene since last epoch $t-1$. As explained earlier, the hypotheses corresponding to disappeared targets are ignored for the purpose of filtering and are not considered for the following observation update (they are not indexed in the set $\mathbb{I}_{t|t-1}$). They will however be useful for track extraction and thus have to be stored.

The approximated multi-target configuration $\mathcal{P}_{t|t-1}$ after prediction from time $t-1$ to time t is then defined as $\mathcal{P}_{t|t-1} = \{p^{\boldsymbol{i}}_{t|t-1}, w^{\boldsymbol{i}}_{t|t-1}, n^{\boldsymbol{i}}_{t|t-1}\}_{\boldsymbol{i}\in\mathbb{I}_{t|t-1}}$. Note that, due to the modelling assumption on the independence of the targets **M.3** and as seen in the prediction equations (13) and (14), the time prediction step applies independently to each hypothesis and thus has a linear complexity w.r.t. the number of hypotheses.

Observation update

The probability that a false alarm will be generated in a given resolution cell $z \in Z'_t$ is denoted v^z_t. For any $\boldsymbol{k} = (t, \boldsymbol{o}) \in \mathbb{I}_{t|t-1}$ and any $z \in \bar{Z}_t$, define $\boldsymbol{i}$ as the index $(t, \boldsymbol{o} \times z)$, with $\boldsymbol{o} \times z$ being the concatenation of $\boldsymbol{o}$ and z, and define $p^{\boldsymbol{i}}_t$ as the probability density function on $\mathbf{X}_t$ characterised by

$$p^{\boldsymbol{i}}_t(x) = \frac{\ell^z_t(x) p^{\boldsymbol{k}}_{t|t-1}(x)}{\int \ell^z_t(x') p^{\boldsymbol{k}}_{t|t-1}(x')\mathrm{d}x'} \tag{15}$$

for any $x \in \mathbf{X}_t$ and let the weights be characterised equivalently by

$$w^{\boldsymbol{i}}_t = \frac{w^{\boldsymbol{k},z}_{\mathrm{ex}} \breve{w}^{\boldsymbol{k},z}_t}{\sum_{z'\in\bar{Z}_t} w^{\boldsymbol{k},z'}_{\mathrm{ex}} w^{\boldsymbol{k},z'}_t} \qquad \text{or} \qquad w^{\boldsymbol{i}}_t = \frac{w^{\boldsymbol{k},z}_{\mathrm{ex}} \breve{w}^{\boldsymbol{k},z}_t}{\sum_{\boldsymbol{k}'\in\mathbb{I}_{t|t-1}} w^{\boldsymbol{k}',z}_{\mathrm{ex}} w^{\boldsymbol{k}',z}_t}, \tag{16}$$

where the scalar $w^{\boldsymbol{k},z}_t = \breve{w}^{\boldsymbol{k},z}_t + \mathbf{1}_\phi(z)(1 - w^{\boldsymbol{k}}_{t|t-1})$ is the probability mass attributed to the association between $\boldsymbol{k}$ and z including the possibility that the target does not actually exist in the case of detection failure. The posterior probability for an observation $z \in Z_t$ to be a false alarm is also obtained via (16) when $\boldsymbol{k} = z$, by setting $w^{z,z}_t = \breve{w}^{z,z}_t = v^z_t$, $w^{z,\phi}_t = 1 - v^z_t$, and $w^{z,z'}_t = 0$ if $z \neq z'$. For any $z \in \bar{Z}_t$ and any $\boldsymbol{k} \in \mathbb{I}_{t|t-1}$ or $\boldsymbol{k} = z$, the scalar $w^{\boldsymbol{k},z}_{\mathrm{ex}}$ is the weight corresponding to the association of the observations in $Z_t \setminus \{z\}$ with false alarms, any of the remaining undetected individuals, or any remaining hypotheses in $\mathbb{I}_{t|t-1} \setminus \{\boldsymbol{k}\}$. This scalar can be expressed as

$$w^{\boldsymbol{k},z}_{\mathrm{ex}} = C'_t(\boldsymbol{k}, z) \prod_{\boldsymbol{k}'\in\mathbb{I}^{\mathrm{m}}_{t|t-1}\setminus\{\boldsymbol{k}\}} \left[w^{\boldsymbol{k}',\phi}_t + \sum_{z'\in Z_t\setminus\{z\}} \frac{w^{\boldsymbol{k}',z'}_t}{C_t(z')} \right], \tag{17}$$

where $C_t(z) = w^{\mathrm{u},z}_t / w^{\mathrm{u},\phi}_t + v^z_t/(1 - v^z_t)$ and where

$$C'_t(\boldsymbol{k}, z) = \left[w^{\mathrm{u},\phi}_t\right]^{n^{\mathrm{u}}_{t|t-1} - \mathbf{1}_{\mathrm{u}}(\boldsymbol{k})} \left[\prod_{z'\in Z_t\setminus Z'} (1 - v^{z'}_t) \right] \left[\prod_{z'\in Z_t\setminus\{z\}} C_t(z') \right] \tag{18}$$

with $Z' = \emptyset$ when $\boldsymbol{k} \in \mathbb{I}_{t|t-1}$ and $Z' = \{z\}$ when $\boldsymbol{k}$ corresponds to a false alarm ($\boldsymbol{k} = z$). Note that the hypotheses corresponding to false alarms are ignored for the purpose of filtering and are not considered for the next time step (they are not indexed in the set $\mathbb{I}_t$). They will however be useful for track extraction and thus have to be stored.

The approximated multi-target configuration $\mathcal{P}_t$ after the observation update at time t is then equal to $\{p^{\boldsymbol{i}}_t, w^{\boldsymbol{i}}_t, n^{\boldsymbol{i}}_t\}_{\boldsymbol{i}\in\mathbb{I}_t}$ where $n^{\boldsymbol{i}}_t = n^{\mathrm{u}}_{t|t-1}$ if $\boldsymbol{i} = \mathrm{u}$ and $n^{\boldsymbol{i}}_t = 1$ otherwise. The assumptions **S.2** and **S.3** are the key elements that lead to the structure of the posterior weights (16), (17) of the hypotheses. In particular, the computation of the weight $w^{\boldsymbol{k},z}_{\mathrm{ex}}$ does not involve combinatorial operations on the subsets of observations and/or hypotheses. The data update step thus has a linear complexity w.r.t. the number of hypotheses and the number of observations.

IMPLEMENTATION OF THE HISP FILTER FOR A SSA SCENARIO

Generation of the ground truth

The space of interest is assumed constant and corresponds to a volume of space centred on Earth (see Figure 2), in which there are 30 orbiting objects with initial state as given in Table 1. The orbits are created utilizing a Runge-Kutta $7/8$ numerical integration. The Earth gravitational field is taken into account up to order and degree 12; third body perturbations of the Sun, the Moon, and direct radiation pressure were considered as well. Also, spherical shapes are assumed for the orbiting objects.

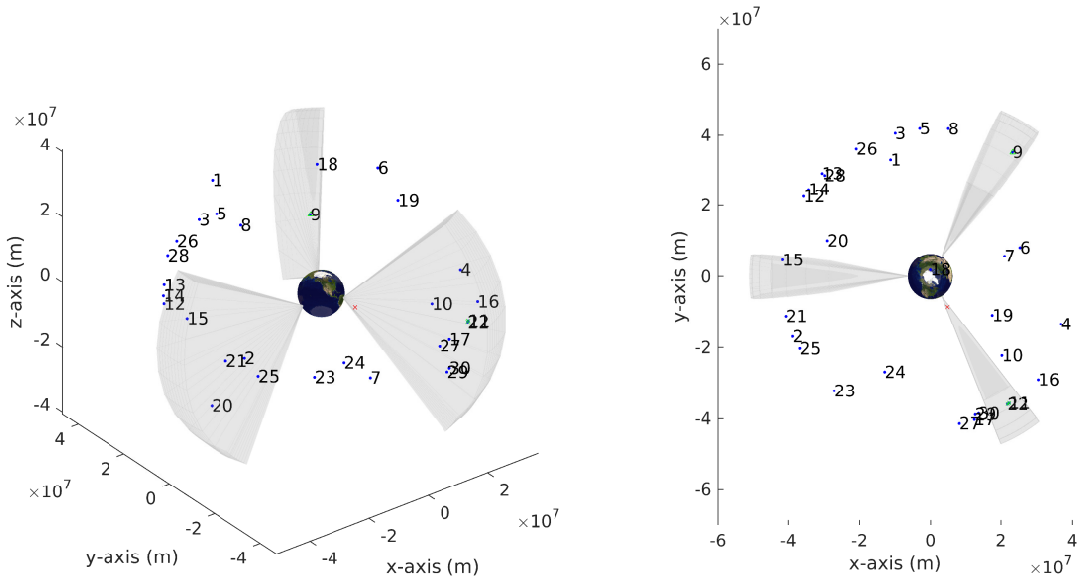

Figure 2: The near-Earth space with the initial position of the 30 targets (blue dots) and the sensor FoVs (grey volumes), in 3D view (left) and 2D view from above (right).

Target state space and probability densities

Instead of Cartesian coordinates as in our previous work in the context of SSA,[19,20,28,29] we use orbital elements to allow for a more natural representation of the prediction kernel representing the orbital motion model. A target state $x \in \mathbf{X}_t^{\bullet} \subseteq \mathbb{R}^6$ describes the set of orbital elements $[\Omega, \omega, i, a, e, M]^T$ representing the right ascension of the ascending node Ω, the argument of perigee ω, the inclination i, the semi-major axis a, the eccentricity e, and the mean anomaly M.[24] The probability densities on $\mathbf{X}_t^{\bullet}$, describing the spatial distribution of the hypotheses, are implemented through a Sequential Monte Carlo (SMC) approach.[30] More specifically, a probability density $p_t^{\boldsymbol{i}}$ on $\mathbf{X}_t^{\bullet}$ is approximated by a set of J weighted particles $\{\gamma_t^{\boldsymbol{i},j}, x_t^{\boldsymbol{i},j}\}_{j=1}^{J}$ such that

$$p_t^{\boldsymbol{i}}(\cdot) \simeq \sum_{j=1}^{J} \gamma_t^{\boldsymbol{i},j} \delta_{x_t^{\boldsymbol{i},j}}(\cdot), \tag{19}$$

where δ_x denotes the Dirac delta function in x, and with $\sum_{j=1}^{J} \gamma_t^{\boldsymbol{i},j} = 1$.

Table 1: Initial semi-major axis a, eccentricity e, inclination i, right ascension of the ascending node Ω, argument of perigee ω, and true anomaly ν of the 30 orbiting objects in the scenario, sorted by track ID.

ID	a (km)	e	i (°)	Ω (°)	ω (°)	ν (°)	ID	a (km)	e	i (°)	Ω (°)	ω (°)	ν (°)
1	42170.23	0.000973	35.74	359.30	124.11	341.97	16	42165.90	0.000333	0.0258	109.85	105.54	227.60
2	42190.79	0.000492	2.64	295.41	255.24	317.11	17	42165.04	0.000341	0.0247	174.29	347.57	254.69
3	42164.04	0.000724	2.44	295.04	203.94	90.98	18	24727.66	0.716	1.00	106.26	59.20	146.90
4	42153.98	0.000899	4.64	302.39	221.78	44.81	19	42165.57	0.000470	0.0215	242.27	354.11	65.60
5	42292.17	0.000292	14.44	339.69	146.81	352.69	20	42166.58	0.000146	0.0240	214.79	359.35	282.24
6	42164.64	0.000141	13.88	100.70	16.65	163.95	21	42166.67	0.000166	0.0515	123.26	79.71	301.46
7	42212.84	0.000733	14.93	10.88	178.06	306.36	22	42164.80	0.00157	7.43	52.77	114.58	6.10
8	42359.18	0.000915	15.02	14.21	94.00	179.74	23	42165.97	0.000279	0.0283	89.19	131.19	96.03
9	42249.35	0.000779	14.17	27.57	160.13	102.09	24	42165.37	0.000269	0.0332	236.95	21.52	28.76
10	42308.74	0.000319	13.81	30.98	346.16	386.31	25	24738.09	0.721	88.19	313.00	287.64	164.39
11	42415.51	0.000439	11.59	41.16	175.70	247.43	26	24637.14	0.687	64.85	186.72	272.84	205.14
12	24520.92	0.718	6.54	166.94	338.94	193.98	27	42170.58	0.00345	54.43	203.14	195.94	106.66
13	42525.07	0.000697	10.94	42.45	109.67	302.51	28	42166.40	0.000668	2.72	245.36	327.12	342.87
14	24937.89	0.710	63.00	227.43	288.57	199.96	29	42165.96	0.000378	0.0310	31.02	188.23	81.98
15	42165.47	0.000381	63.00	72.85	158.97	127.09	30	24353.42	0.725	17.85	272.76	181.96	148.44

Prediction step

While the orbital trajectories composing the ground truth account for physical perturbations and are generated offline, the prediction model used by the HISP filter assumes an unperturbed motion model for the sake of simplicity and computational efficiency. More specifically, a SMC particle $x_{t-1} = [\Omega, \omega, i, a, e, M]^T_{t-1}$ representing a target state at time $t-1$ evolves to a SMC particle $x_t = [\Omega, \omega, i, a, e, M]^T_t$ at time t through the transition kernel q^π_t as follows [24, p.488]

$$x_t = x_{t-1} + \Delta_t \begin{bmatrix} \mathbf{0}_{5,1} \\ n_{t-1} \end{bmatrix} + W, \tag{20}$$

where Δ_t is the time lapse between time $t-1$ and t, $\mathbf{0}_{j,k}$ the null matrix of size $j \times k$, $n_{t-1} = \sqrt{\mu_\mathrm{e}/a^3_{t-1}}$, with μ_e being the standard gravitational parameter of Earth, is the mean motion of particle x_{t-1}. The vector $\mathrm{W} \sim \mathcal{N}(\cdot; 0, Q_t)$ is Gaussian noise with zero mean and covariance Q_t, accounting for the modelling mismatches which are bound to occur due to the simplified transition kernel. Considering the extreme sensitivity of orbital trajectories to slight changes on the orbital elements, a simple prediction model such as (20) must be parametrized with very little noise to prevent an excessive spreading of the particle cloud while the targets are outside the sensor FoVs. In order to add diversity to the particles in the orbital plane, the standard deviation of the Gaussian noise is set to $\sigma_a = \Delta_t \times 10^{-10}\mathrm{m}$ on the semi-major axis component, $\sigma_e = \Delta_t \times 10^{-10}$ on the eccentricity component, and zeros elsewhere.

The disappearance of targets due to specific orbital behaviours (e.g. targets disintegrating in the atmosphere, or leaving near-Earth space) is out of the scope of this paper. The disappearance kernel q^ω_t is assumed constant and verifies, for any $x \in \mathbf{X}^\bullet_t$, $q^\omega_t(x, \psi) = 10^{-10}$ (i.e. the probability of survival p^π_t of the targets is almost one).

Sensors

The three sensors in the scenario share the same model, a radar with Doppler effect. An observation $z \in \mathbf{Z}^\bullet_t \subseteq \mathbb{R}^4$ is radar-attributable vector $[r, \theta, \varphi, \dot{r}]^T$ in the spherical frame centred on the sensor. The sensor resolution and FoV profile are given in Table 2. The probability of detection is uniform in the FoV, and set to a constant value of $p_\mathrm{d} = 0.98$. The false positives are independently identically distributed (i.i.d.) in the sensor FoV, and the number of false positives per sensor and per time step is Poisson-distributed with mean 1 (false alarm rate of $v^z_t = 7.7 \times 10^{-15}$).

The sensors are located at latitudes of $15°$, $0°$, and $-15°$ and evenly spread in longitude. Each sensor sweeps along the parallel of latitude on a $120°$ arc at an angular speed of $\frac{2\pi}{5000}\mathrm{rad\,s^{-1}}$, providing a reasonable coverage of the near-Earth space (see Figure 2).

Table 2: Sensor resolution and field of view profile

	Range r (m)	Azimuth θ ($^\circ$)	Elevation φ ($^\circ$)	Range rate $\dot{r}$ ($\mathrm{m\,s^{-1}}$)
Cell resolution	100	0.1	0.1	10
Noise (std. dev.)	100	0.1	0.1	10
Field of view	$[50\ \ 45\times10^6]$	$[-8\ \ 8]$	$[-45\ \ 45]$	$[-1\times10^4\ \ 1\times10^4]$

Data update step

The single-object data correction step requires specific consideration in the context of SSA. A straightforward implementation of the single-Bayes update step (15) would lead to a particle correction mechanism of the form

$$\gamma_t^{\boldsymbol{i},j} = \frac{\ell_t^z(x_{t|t-1}^{\boldsymbol{k},j})\gamma_{t|t-1}^{\boldsymbol{k},j}}{\sum_{j'=1}^{J}\ell_t^z(x_{t|t-1}^{\boldsymbol{k},j'})\gamma_{t|t-1}^{\boldsymbol{k},j'}}, \tag{21}$$

updating the particle distribution $\{\gamma_{t|t-1}^{\boldsymbol{k},j}, x_{t|t-1}^{\boldsymbol{k},j}\}_{j=1}^{J}$ of the predicted hypothesis $\boldsymbol{k}\in\mathbb{I}_{t|t-1}$ to the particle distribution $\{\gamma_t^{\boldsymbol{i},j}, x_t^{\boldsymbol{i},j}\}_{j=1}^{J}$ of the updated hypothesis $\boldsymbol{i}\in\mathbb{I}_t$. This solution, however, often leads to particle degeneracy, especially when a target is re-entering a sensor FoV after a long time without data correction and the particle cloud of the corresponding hypothesis has inflated in the target state space.[29] In this paper we exploit a data update mechanism inspired from previous works on cameras,[31] that we exploited in the context of SSA in[19,20,28] and explained in more details in.[29]

Let us assume that the previously-detected hypothesis $\boldsymbol{k}\in\mathbb{I}_{t|t-1}^{\mathrm{m}}$, with particle distribution $\{\gamma_{t|t-1}^{\boldsymbol{k},j}, x_{t|t-1}^{\boldsymbol{k},j}\}_{j=1}^{J}$ and probability of existence $w_{t|t-1}^{\boldsymbol{k}}$, needs to be updated following its association with the (possibly empty) observation $z\in\bar{Z}_t$, to form the updated hypothesis $\boldsymbol{i}\in\mathbb{I}_t^{\mathrm{m}}$. The special case $z=\phi$ (i.e., the corresponding target is not detected this time step) is straightforward as it does not involve likelihoods of associations l_t^z causing particle degeneracy. Substituting (9) into (21) yields, for any $j\in[1\ J]$:

$$\gamma_t^{\boldsymbol{i},j} = \frac{\big[1-p_{\mathrm{d},t}(x_{t|t-1}^{\boldsymbol{k},j})\big]\gamma_{t|t-1}^{\boldsymbol{k},j}}{\sum_{j'=1}^{J}\big[1-p_{\mathrm{d},t}(x_{t|t-1}^{\boldsymbol{k},j'})\big]\gamma_{t|t-1}^{\boldsymbol{k},j'}}, \tag{22}$$

and the association weight (10) becomes

$$\breve{w}_t^{\boldsymbol{k},\phi} = w_{t|t-1}^{\boldsymbol{k}}\sum_{j=1}^{J}\big[1-p_{\mathrm{d},t}(x_{t|t-1}^{\boldsymbol{k},j})\big]\gamma_{t|t-1}^{\boldsymbol{k},j}. \tag{23}$$

Let us now suppose that $z\in Z_t$ – that is, the corresponding target is detected and needs to be corrected accordingly. The principle of the data update mechanism is to perform the correction step in the spherical frame centred on the sensor or *extended observation space*, motivated by the facts that:[29]

1. The nature of the orbital trajectories being such that the confidence region spreads along the orbit in an arc shape, a single-object probability density $p_{t|t-1}^{\boldsymbol{k}}$ *projected in the extended observation space* can be reasonably approximated as a Gaussian distribution,
2. The components of a radar-attributable vector $[r,\theta,\varphi,\dot{r}]^T$ being spherical coordinates augmented with Gaussian noise, the observation process is linear Gaussian in the extended observation space.

In consequence, the probability density $p_{t|t-1}^{\boldsymbol{k}}$ of the predicted hypothesis can be corrected in the extended observation space through a classical Kalman update[32] through the following steps:

1. Transform the predicted distribution $p^{\boldsymbol{k}}_{t|t-1}$, weighted with the probability of detection, in the spherical frame centred on the sensor: $\{\gamma^{\boldsymbol{k},j}_{t|t-1}, x^{\boldsymbol{k},j}_{t|t-1}\}_{j=1}^{J} \to \{\gamma^{\boldsymbol{k},j}_{t|t-1} p_{\mathrm{d},t}(x^{\boldsymbol{k},j}_{t|t-1}), s^{\boldsymbol{k},j}_{t|t-1}\}_{j=1}^{J}$,
2. Produce the Gaussian approximation of the resulting cloud: $\{\gamma^{\boldsymbol{k},j}_{t|t-1} p_{\mathrm{d},t}(x^{\boldsymbol{k},j}_{t|t-1}), s^{\boldsymbol{k},j}_{t|t-1}\}_{j=1}^{J} \to (\mu^{\boldsymbol{k}}_{t|t-1}, P^{\boldsymbol{k}}_{t|t-1})$,
3. Update the resulting distribution with observation z, using a Kalman update step: $(\mu^{\boldsymbol{k}}_{t|t-1}, P^{\boldsymbol{k}}_{t|t-1}) \to (\mu^{\boldsymbol{i}}_{t}, P^{\boldsymbol{i}}_{t})$,
4. Sample the resulting distribution: $(\mu^{\boldsymbol{i}}_{t}, P^{\boldsymbol{i}}_{t}) \to \{J^{-1}, s^{\boldsymbol{i},j}_{t}\}_{j=1}^{J}$,
5. Transform back the particle cloud to the sets of orbital elements: $\{J^{-1}, s^{\boldsymbol{i},j}_{t}\}_{j=1}^{J} \to \{J^{-1}, x^{\boldsymbol{i},j}_{t}\}_{j=1}^{J}$.

The probability density $p^{\boldsymbol{i}}_t$ of the updated hypothesis is then approximated by the particle cloud $\{J^{-1}, x^{\boldsymbol{i},j}_{t}\}_{j=1}^{J}$. Adapting the integral (8) to the multivariate case, the association weight (10) becomes

$$\breve{w}^{\boldsymbol{k},z}_{t} = w^{\boldsymbol{k}}_{t|t-1} \left[\sum_{j=1}^{J} p_{\mathrm{d},t}(x^{\boldsymbol{k},j}_{t|t-1}) \gamma^{\boldsymbol{k},j}_{t|t-1} \right] \sqrt{\frac{|R|}{|S^{\boldsymbol{k}}_{t|t-1}|}} \exp\left(-\frac{1}{2} (H\mu^{\boldsymbol{k}}_{t|t-1} - z)^T (S^{\boldsymbol{k}}_{t|t-1})^{-1} (H\mu^{\boldsymbol{k}}_{t|t-1} - z) \right), \quad (24)$$

where $|\cdot|$ is the determinant, $H = [\boldsymbol{I}_4 \ \boldsymbol{0}_{4,2}]$ is the observation matrix of the sensor, with $\boldsymbol{I}_n$ the identity matrix of size n, $R = \mathrm{diag}([\sigma_r^2, \sigma_\theta^2, \sigma_\varphi^2, \sigma_{\dot{r}}^2])$ is the noise covariance matrix of the sensor, and $S^{\boldsymbol{k}}_{t|t-1} = H P^{\boldsymbol{k}}_{t|t-1} H^T + R$ is the innovation covariance.

Initial orbit determination

Let us now assume that an individual of the sub-population of yet-to-detected targets u is to become detected for the first time through observation $z \in Z_t$ to form the hypothesis $\boldsymbol{i} \in \mathbb{I}^{\mathrm{m}}_t$. Since we assume no prior knowledge on the orbiting objects, the probability density $p^{\mathrm{u}}_{t|t-1}$ carries little information on the state of the yet-to-be-detected targets, save that they are orbiting around Earth. Similarly to our previous implementations in the context of SSA,[19,20,28] we adopt the *admissible region* approach[33] to find admissible values for the unobserved angular rates $(\dot{\theta}, \dot{\varphi})$ from the radar-attributable vector $z = [r, \theta, \varphi, \dot{r}]^T$. A yet-to-be-detected target is orbiting around Earth; its internal energy is non-positive and we can write[34,35]

$$\frac{1}{2}|\dot{\mathbf{r}}|^2 - \frac{\mu_e}{|\mathbf{r}|} \leq 0, \quad (25)$$

where $\mathbf{r}$ is the geocentric inertial position vector of the target, i.e.

$$\mathbf{r} = \mathbf{r}_{\mathrm{s}} + r\boldsymbol{\rho}_{\mathrm{r}} \qquad \text{and} \qquad \dot{\mathbf{r}} = \dot{\mathbf{r}}_{\mathrm{s}} + \dot{r}\boldsymbol{\rho}_{\mathrm{r}} + r\dot{\theta}\boldsymbol{\rho}_{\theta} + r\dot{\varphi}\boldsymbol{\rho}_{\varphi}, \quad (26)$$

where $\mathbf{r}_{\mathrm{s}}$ is the geocentric inertial position vector of the sensor, and $\boldsymbol{\rho}_{\mathrm{r}}, \boldsymbol{\rho}_{\theta}, \boldsymbol{\rho}_{\varphi}$ the unit vectors associated to the observation $[r, \theta, \varphi, \dot{r}]^T$. Substituting (26) into (25) yields

$$\alpha_1 \dot{\theta}^2 + \alpha_2 \dot{\varphi}^2 + \alpha_3 \dot{\theta} + \alpha_4 \dot{\varphi} + \alpha_5 \leq 0, \quad (27)$$

with the parameters α_i given by

$$(\alpha_1, \ldots, \alpha_5) = \left(r^2 \cos^2\varphi, \quad r^2, \quad \frac{r\dot{\mathbf{r}}_{\mathrm{s}} \cdot \boldsymbol{\rho}_{\theta}}{2}, \quad \frac{r\dot{\mathbf{r}}_{\mathrm{s}} \cdot \boldsymbol{\rho}_{\varphi}}{2}, \quad \dot{r}^2 + 2\dot{r}\dot{\mathbf{r}}_{\mathrm{s}} \cdot \boldsymbol{\rho}_{\mathrm{r}} + |\dot{\mathbf{r}}_{\mathrm{s}}|^2 - \frac{2\mu}{\sqrt{r^2 + 2r\mathbf{r}_{\mathrm{s}} \cdot \boldsymbol{\rho}_{\mathrm{r}} + |\mathbf{r}_{\mathrm{s}}|^2}} \right).$$

From the internal energy equation (27), the boundaries of the admissible region for $(\dot{\theta}, \dot{\varphi})$ are found to be:[33]

$$\dot{\theta} = \frac{\alpha_3}{\alpha_1} + \sqrt{\frac{\alpha_3^2}{\alpha_1^2} + \frac{\alpha_4^2}{\alpha_1 \alpha_2} - \frac{\alpha_5}{\alpha_1}} \cos\phi \qquad \text{and} \qquad \dot{\varphi} = \frac{\alpha_4}{\alpha_2} + \sqrt{\frac{\alpha_3^2}{\alpha_1 \alpha_2} + \frac{\alpha_4^2}{\alpha_2^2} - \frac{\alpha_5}{\alpha_2}} \sin\phi, \quad (28)$$

with $\phi \in [0, 2\pi)$. The initial particle distribution $\{J^{-1}, s^{\boldsymbol{i},j}_{t}\}_{j=1}^{J}$ can then be sampled from (28) for the unobserved components $(\dot{\theta}, \dot{\varphi})$, and sampled from the Gaussian distribution $\mathcal{N}(\cdot; z, R)$ for the observed components. Then, the particles are transformed to the sets of orbital elements to produce the approximation $\{J^{-1}, x^{\boldsymbol{i},j}_{t}\}_{j=1}^{J}$ of the probability density $p^{\boldsymbol{i}}_t$ of the updated hypothesis $\boldsymbol{i} \in \mathbb{I}_t$.

Track extraction

In this section, we propose a method to extract tracks from the multi-target configuration $\mathcal{P}_t = \{p_t^{\boldsymbol{i}}, w_t^{\boldsymbol{i}}, n_t^{\boldsymbol{i}}\}_{\boldsymbol{i}\in\mathbb{I}_t}$ propagated by the HISP filter, that is, to extract the subset of hypotheses that is the likeliest candidate to represent the population of objects in the scene. Note that the track extraction process has no influence on the filtering process, as the operations described in the next paragraph are for the purpose of extraction only and do not modify the multi-target configuration $\mathcal{P}_t$, to be processed as it is during the next time step.

Recall from the simplifying assumption **S.3** and the data update step of the filter that the probabilities of existence of the hypotheses are marginalized over the population, and thus do not provide insight on the *joint* existence of subsets of hypotheses. The observation paths do, however, since according to the modelling assumption **M**.2 targets do not share observations. A simple and efficient track extraction method is therefore to select the subset of hypotheses with the highest possible weights *and* whose observation paths agree with the observations collected during some sliding time window. Since all the observations collected in this time window must be explained, the posterior probabilities for each observation produced during this time window to be false positives are computed and stored as hypotheses, along with hypotheses corresponding to targets that disappeared during the time window. The track extraction can then be solved through the following optimisation problem

$$\operatorname{argmax}_{I\subseteq\tilde{\mathbb{I}}_t} \prod_{\boldsymbol{i}\in I} w_t^{\boldsymbol{i}}, \tag{29}$$

where $\tilde{\mathbb{I}}_t$ is the temporary set of hypotheses resulting from the modifications above, and under the conditions a) the union of all observation paths over the time window $T \subseteq \mathbb{T}\cap[0,t]$ must contain all the observations over this window, and b) the observation paths in I must be pairwise compatible (each observation cannot be used more than once). The solution to this problem is the same as the one for

$$\operatorname{argmax}_{I\subseteq\tilde{\mathbb{I}}_t} \sum_{\boldsymbol{i}\in I} \log w_t^{\boldsymbol{i}} \tag{30}$$

with the same constraints since all $w_t^{\boldsymbol{i}}$ are strictly positive. The latter problem can be solved by integer programming*. Hypotheses that are not associated to any observations during the time window are deemed as non-conflicting and are extracted on an individual basis, when their weight exceeds some threshold τ_{d}.

Pruning and merging

We present in this section simplifying techniques that aim to reduce the memory and computational requirements of the HISP filter incurring a reasonable information loss. In the general case, we have seen earlier that the output of the filter at time $t-1$ is a multi-target configuration $\mathcal{P}_{t-1}$ equal to $\{p_{t-1}^{\boldsymbol{i}}, w_{t-1}^{\boldsymbol{i}}, n_{t-1}^{\boldsymbol{i}}\}_{\boldsymbol{i}\in\mathbb{I}_{t-1}}$. One can note that:

1. A hypothesis $\boldsymbol{i} \in \mathbb{I}_{t-1}$ may have a negligible weight $w_{t-1}^{\boldsymbol{i}}$ – for example, a hypothesis assuming no detections for several successive time steps while the corresponding target is in a sensor FoV. Such a hypothesis can be *pruned* from memory with little to no cost on performance, since it is very likely never to be credible enough to be confirmed as track.
2. Some hypotheses $I \subseteq \mathbb{I}_{t-1}$ may have probability densities $p_{t-1}^{\boldsymbol{i}}$, $i \in I$, that are very "close" to each other – for example, two hypotheses whose observation path only differ on their association in a single, distant time step in the past, and thus likely to maintain very close probability densities. Such probability densities can be *merged* in memory with little to no cost on performance, since by construction they represent very similar information.
3. Some hypotheses $I \subseteq \mathbb{I}_{t-1}$ may have the same observation path over the extraction window T so that they can be assumed to represent the same potential target and can be merged into a single hypothesis which weight is $w = \sum_{\boldsymbol{i}\in I} w_t^{\boldsymbol{i}}$ if $w \leq 1$ only – since hypotheses cannot have a weight strictly greater than 1. This procedure has for

*Using for instance the GNU Linear Programming Kit (GLPK).

consequence that the resulting hypothesis is more likely to be selected in the track extraction and that the total number of hypotheses is reduced.

Let $\bar{\mathbb{J}}_{t-1}$ be the subset of indices in $\mathbb{I}_{t-1}$ that have been retained at time $t-1$. After time predication and observation update, the corresponding set of indices is denoted $\mathbb{J}_t$, which is a subset of $\mathbb{I}_t$ by construction. To avoid propagating distributions that are very "close" to each other, several hypotheses in $\bar{\mathbb{J}}_{t-1}$ can be allowed to use the same probability density (addressing the point 2 above), so that all probability densities can be indexed by a set $\bar{\mathbb{L}}_{t-1}$ made of subsets of $\bar{\mathbb{J}}_{t-1}$. In other words, each probability density is indexed by the set of hypotheses associated with it. To be well defined, $\bar{\mathbb{L}}_{t-1}$ has to be a partition of $\bar{\mathbb{J}}_{t-1}$; that is, a probability density should be associated to at least one hypothesis, and a hypothesis should not be associated to more than one probability density.

After time prediction and observation update, the corresponding set is denoted $\mathbb{L}_t$. Each index L in $\mathbb{L}_t$ is given a weight w_t^L defined as

$$w_t^L = \sum_{\boldsymbol{j} \in L} w_t^{\boldsymbol{j}}, \tag{31}$$

that is, the weight of a probability density is the sum of the weights of all the hypotheses associated to it. Selecting candidates for merging will require the comparison of probability densities p_t^L, $L \in \mathbb{L}_t$, which are approximated as weighted particle sets $\{\gamma_t^{L,j}, x_t^{L,j}\}_{j=1}^J$ on the space of orbital elements $\mathbf{X}_t^\bullet$. For the sake of simplicity, the "closeness" between these probability densities will be assessed through their projection in the spherical frame centred on Earth, where they can be reasonably approximated by Gaussian distributions $\mathcal{N}(\mu_t^L, P_t^L)$.

The following simplifications are then applied to $\mathbb{J}_t$ and $\mathbb{L}_t$:

S.4 *Pruning:* Retain the subset $\hat{\mathbb{J}}_t$ of hypotheses $\boldsymbol{j} \in \mathbb{J}_t$ such that $w_t^{\boldsymbol{j}} > \tau_\mathrm{p}$ and update $\mathbb{L}_t$ by removing the indices of discarded hypotheses.

S.5 *Merging of distributions:* Define a partition $\bar{\mathbb{L}}_t$ of $\hat{\mathbb{J}}_t$ in the following way:

(i) Define $\bar{\mathbb{L}}_t = \emptyset$ and $K = \emptyset$,

(ii) Find the index of highest weight $L = \mathrm{argmax}_{L' \in \mathbb{L}_t \setminus K} w_t^{L'}$ and define K' as the set containing all the indices L' such that the Mahalanobis distance between the corresponding distributions $\mathcal{N}(\mu_t^L, P_t^L)$ and $\mathcal{N}(\mu_t^{L'}, P_t^{L'})$ is less than a given threshold τ_m. Define K'' as the union of these indices so that $K'' \subseteq \hat{\mathbb{J}}_t$,

(iii) Sample from the particle clouds $\{w_t^L \gamma_t^{L,j} (\sum_{L' \in K'} w_t^{L'})^{-1}, x_t^{L,j}\}_{j=1}^J$, $L \in K'$, to form the new merged probability density $p_t^{K'}$,

(iv) Redefine K as $K \cup K'$ and $\bar{\mathbb{L}}_t$ as $\bar{\mathbb{L}}_t \cup \{K''\}$,

(v) Return to step (ii) until $K = \mathbb{L}_t$.

S.6 *Merging of hypotheses:* Define the subset $\bar{\mathbb{J}}_t$ of $\hat{\mathbb{J}}_t$ of merged hypotheses in the following way:

(i) Define $\bar{\mathbb{J}}_t = \emptyset$ and $K = \emptyset$,

(ii) Find the index of highest weight $\boldsymbol{j} = \mathrm{argmax}_{\boldsymbol{k} \in \hat{\mathbb{J}}_t \setminus K} w_t^{\boldsymbol{k}}$ and define K' as the set containing all the indices $\boldsymbol{k}$ such that the observation paths associated with $\boldsymbol{j}$ and $\boldsymbol{k}$ are the same over the extraction window T. Let $w = \sum_{\boldsymbol{j} \in K'} w_t^{\boldsymbol{j}}$,

(iii) Redefine K as $K \cup K'$,

(iv) If $w \leq 1$ then redefine $\bar{\mathbb{J}}_t$ as $\bar{\mathbb{J}}_t \cup \{\boldsymbol{j}\}$ and $w_t^{\boldsymbol{j}} = w$, otherwise redefine $\bar{\mathbb{J}}_t$ as $\bar{\mathbb{J}}_t \cup K'$,

(v) Return to step (ii) until $K = \hat{\mathbb{J}}_t$.

Simplifying assumptions **S**.4 to **S**.6 allow for reducing the computational cost of the filter while preserving the relevant information and enabling track extraction as introduced in the previous section.

SIMULATION RESULTS

Parametrization of the filter

We assume no prior information on the size of the population to be estimated, that is, the number and the states of all the orbiting targets must be jointly estimated from the collected observations. The average number of appearing targets per time step is set to 10^{-3}. This number is then divided uniformly across sensors and resolution cells to give the probability w_t^α that any potential observation represents an appearing target. The distribution p_t^α is uninformative since nothing is known about the appearing targets before the first observation. The distribution after the first observation is determined by the initial orbit determination. Also, in practice, the probability of detection for appearing targets is set to one so that the set of undetected targets is renewed at every iteration. The shape and size of the admissible region for radar-attributable vectors (28) are relatively easy to handle for a sensor profile as given in Table 2, so that the size of the particle clouds representing single-object probability densities can be set at $J = 500$.

Since the merging of probability densities induces a loss in the quality of the tracks, and considering that our orbital predictor model is relatively poor and targets are often out of the sensor FoVs, we decided for a conservative approach and set the merging threshold τ_m to 5% (confidence region on the Mahalanobis distance) in order to limit the extent of merging operations. The pruning threshold τ_m is set at 10^{-4}. Since the data association is moderately ambiguous in the context of SSA, the most credible hypotheses have few conflicting data associations in their observation paths and the size of the time window T can be set to low values – that is, it is not necessary to check far away in the past to see if two good candidates for track extraction share observations. We nonetheless follow a cautious approach: the size of the window T is set to 10, and the display threshold τ_d (for hypotheses unobserved in the time window) is set to 0.75.

A practical problem in the implementation of the HISP filter in the context of SSA is the presence of "ghost tracks", i.e., hypotheses that are initialized upon a single observation, and never observed for the rest of the scenario – typically, when the origin observation was a false positive on the edges of the FoV. The probability of existence of such hypotheses is low enough and will never be reassessed since their associations to observations will be extremely unlikely at best. Therefore, they will never be considered in the track extraction procedure and will not impact the performance of the filter; however, the growing size of their particle cloud is prone to cause numerical instabilities in our Matlab® implementation. For these reasons, such hypotheses are discarded if they are not observed at least once in the 10 time steps following the initial orbit determination procedure. To avoid further numerical instability in the storage of particle clouds representing probability densities in Matlab®, a measurement gating with a confidence threshold of 99.99% is implemented in order to discard the hypotheses resulting from extremely unlikely data associations.

Results

The scenario is run 1000 time steps with a constant time lapse of $\Delta_t = 20\,\mathrm{s}$ between two successive times steps, thus for a total scenario length of about $5\,\mathrm{h}30\,\mathrm{min}$.

Figure 3 depicts the estimation of the number of objects across the scenario. It shows that the HISP filter is very reactive to the detection of a new object, and takes about two time steps to confirm it as a track. This is not surprising since, considering the volume of the sensor FoVs and the relative scarcity of false positives in the context of SSA, the probability of existence of a hypothesis increases dramatically through successive data associations. One can note two discrepancies around epochs 250 and 850. This is due to a target being represented by two tracks for a brief period of time, and will be discussed in more details in the next paragraph.

In order to study the tracking performance on individual objects, individual statistics are produced for each of the 30 objects. The results are depicted in Figure 4 for Object 1 and in Figure 5 for Object 4. The top-left-hand figure shows the number of tracks per object. A track is assigned to the object which produced the first observation in the observation path of the hypothesis*. If several tracks are associated to the same object (see Figure 5, around epoch 850), it produces a mismatches in the global cardinality estimate as seen earlier in Figure 3. In that case, the "best

*If the first observation is a false alarm, the track is called a "false track", though none occurred in this scenario.

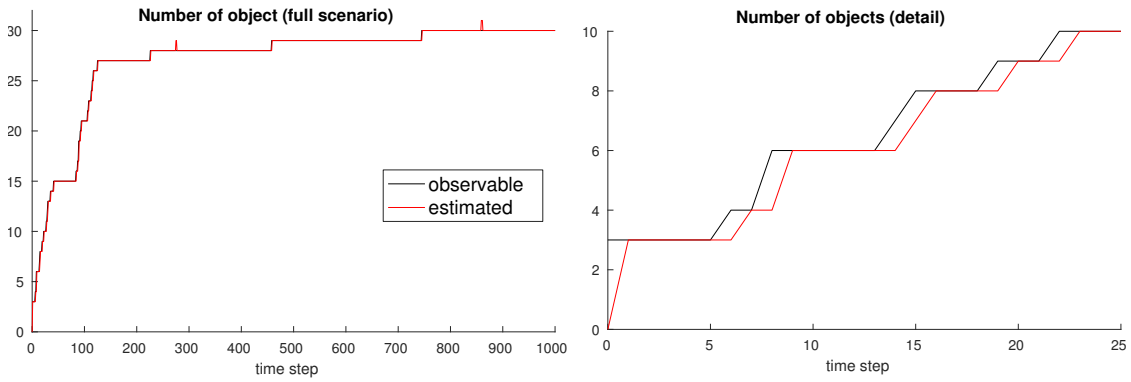

Figure 3: Cardinality estimate, full scenario (left), detail (right). An object is deemed observable from its first time of entry in one of the sensor FoVs, onwards.

track" is defined as the one whose probability density shows the smallest root mean square error (RMSE) w.r.t. the position coordinates of the object in the Earth Centred Inertial (ECI) frame (shown in the bottom-left-hand figure). The bottom-right-hand figure shows the RMSE of the best track w.r.t. the velocity coordinates of the object in the ECI frame. The top-right-hand figure shows the number of track swaps across the scenario. A track swap occurs when the track $\boldsymbol{j} \in \mathbb{I}_t$ representing an object at time t is not a daughter of the track $\boldsymbol{k} \in \mathbb{I}_{t-1}$ representing the same object at time $t-1$, i.e., when the observation paths $\boldsymbol{o}^{\boldsymbol{j}}$, $\boldsymbol{o}^{\boldsymbol{k}}$ are not identical on all their elements until epoch $t-1$ (included). That is, a track swap occurs where the HISP filter "changed its mind" on an object and did not maintain track custody.

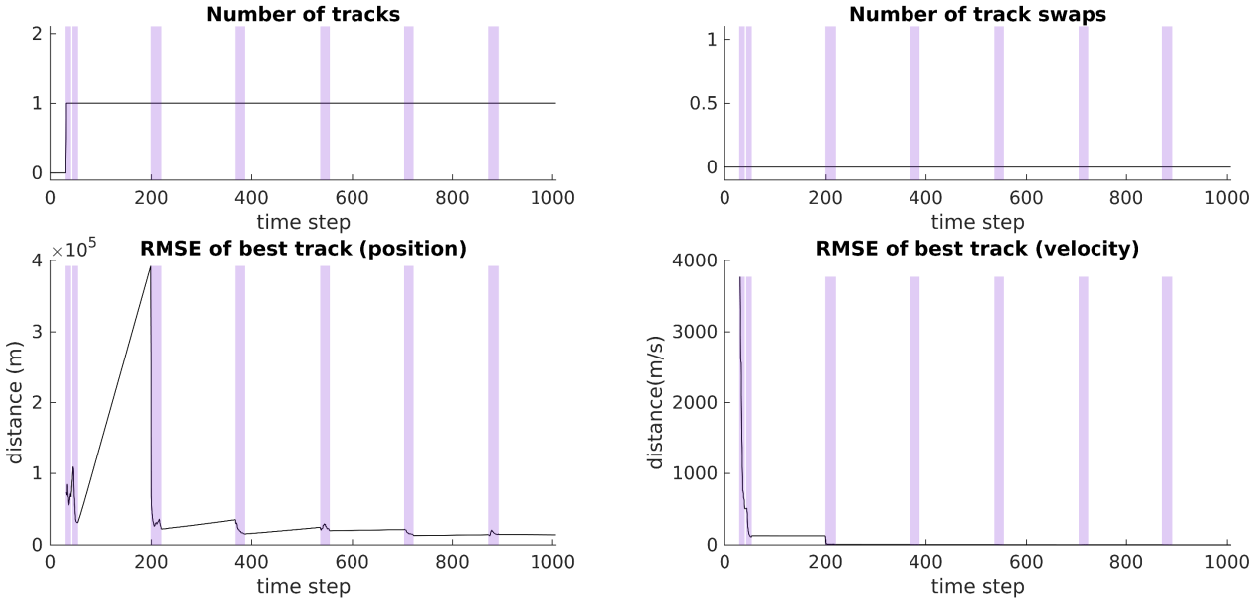

Figure 4: Individual statistics for object 1. The blue areas are time windows where the object is in a the sensor FoVs.

The statistics depicted in Figure 4 denote a situation where the HISP filter shows good reactivity in the detection of the object following its first detection, good stability once the track is confirmed (no track swap across the scenario, and a single track is associated at any time to the object). It also shows an improving tracking accuracy throughout the successive re-entries of the object in the sensor FoVs. All 30 objects but Object 4 and 12 show statistics similar to

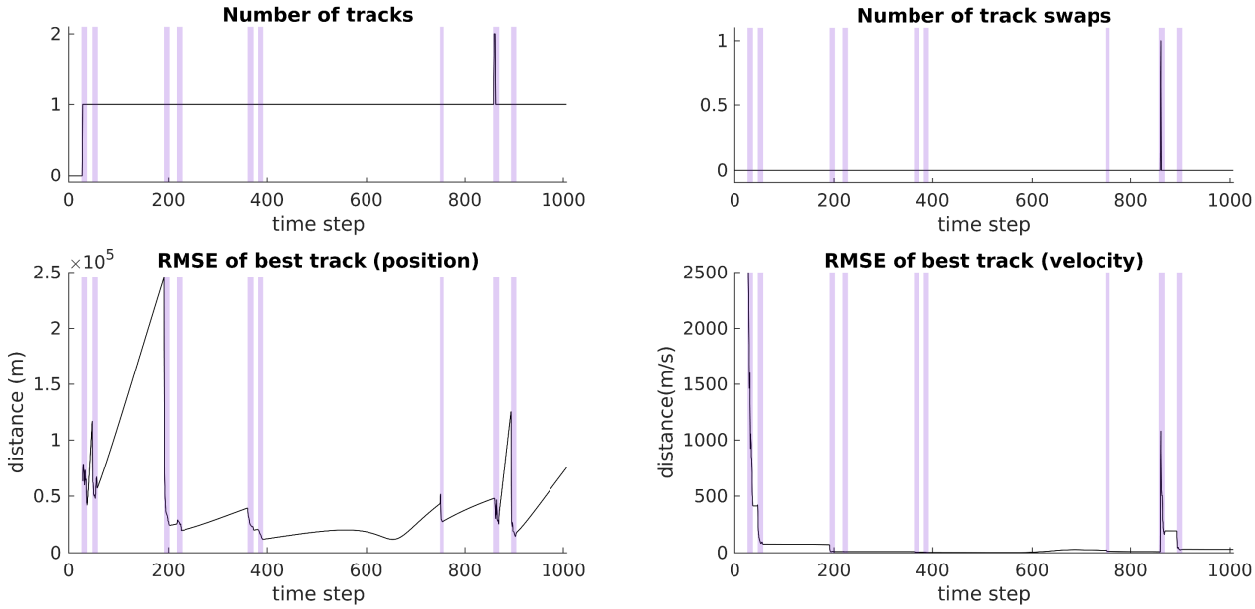

Figure 5: Individual statistics for object 4. The blue areas are time windows where the object is in a sensor FoVs.

Figure 4. The statistics in Figure 5 show a discrepancy during a brief window of time where the HISP filter confirms two tracks for the same object, though quickly swaps to the more recent track while discarding the old one. This situation, shared by Objects 4 and 12, may be explained by the poor accuracy of the prediction model used by the filter. Recall that it does not account for physical perturbations, and thus may induce a growing discrepancy between the track's estimated state and the object's true state. If this discrepancy causes regular failures in the data association, the HISP filter may swap to a more recent track built up from the missed data associations.

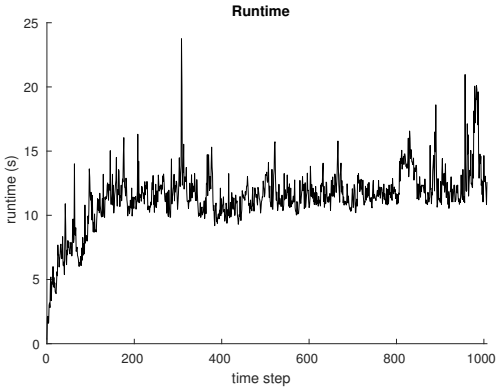

Figure 6: Run time across the scenario (Intel® Core™ i5-6200U @ 2.30GHz).

Figure 6 depicts the run time across the scenario. It shows that the increase in computation time roughly follows the increase in the number of observable objects (see Figure 3), to reach a reasonable value of around 15 s per time step. This trend is expected, since the HISP filter has a linear complexity with the number of hypotheses and observations.

CONCLUSION

This paper presents the HISP filter, a recently developed multi-object detection/tracking algorithm derived from a recent estimation framework for stochastic populations, in the context of SSA. A principled approximation of the DISP filter, illustrated earlier on a SSA scenario, the HISP filter relies on a key additional assumption; namely, the moderate ambiguity in the association between targets and observations, that makes it well-adapted to SSA wide surveillance scenarios. The HISP filtering structure, with linear complexity in the number of propagated hypotheses and the number of collected observations, appears as a promising candidate for detection/tracking problems in large-scale SSA scenarios.

It is tested on a challenging surveillance scenario with 30 targets on various orbits, 3 Doppler radars with limited coverage, missed detections, false alarms, and the absence of prior information on the number and states of the objects of interest. The HISP filter proves reactive in the confirmation of new tracks, shows good performance in maintaining track custody and provides improving tracking performance throughout the successive sensor re-acquisitions of the objects, whilst maintaining a reasonable computational time.

Subsequent works will include the improvement of the single-object Bayesian prediction step through a more accurate orbital motion model including physical perturbations, in order to improve the tracking performances on individual targets.

ACKNOWLEDGEMENTS

Emmanuel Delande, Jose Franco, and Daniel Clark are supported by the Engineering and Physical Sciences Research Council (EPSRC) [Grant Numbers EP/J015180/1 and EP/K014227/1], and the MOD University Defence Research Collaboration (UDRC) in Signal Processing.

REFERENCES

[1] "Space Debris and Human Spacecraft," 2013. http://www.nasa.gov/mission_pages/station/news/orbital_debris.html.

[2] Y. Bar-Shalom, " Tracking methods in a multitarget environment," *Automatic Control, IEEE Transactions on*, Vol. 23, Aug. 1978, pp. 618 – 626.

[3] D. Reid, "An Algorithm for Tracking Multiple Targets," *Automatic Control, IEEE Transactions on*, Vol. 24, No. 6, 1979, pp. 843–854.

[4] W. D. Blair and Y. Bar-Shalom, eds., *Multitarget-Multisensor Tracking: Applications and Advances (Volume III)*. Artech House, 2000.

[5] N. Singh, A. Poore, C. Sheaff, J. Aristoff, and M. K. Jah, "Multiple Hypothesis Tracking (MHT) for Space Surveillance: Results and Simulation Studies," *Advanced Maui Optical and Space Surveillance Technologies Conference*, Sept. 2013, p. E16.

[6] I. R. Goodman, R. P. S. Mahler, and H.-T. Nguyen, *Mathematics of Data Fusion*. Kluwer Academic Publishers, 1997.

[7] R. P. S. Mahler, "Multitarget Bayes Filtering via First-Order Multitarget Moments," *Aerospace and Electronic Systems, IEEE Transactions on*, Vol. 39, No. 4, 2003, pp. 1152–1178.

[8] R. P. S. Mahler, *Statistical Multisource-Multitarget Information Fusion*. Artech House, 2007.

[9] B.-T. Vo and B.-N. Vo, "Labeled Random Finite Sets and Multi-Object Conjuguate Priors," *Signal Processing, IEEE Transactions on*, Vol. 61, No. 13, 2013, pp. 3460–3475.

[10] I. I. Hussein, K. J. DeMars, C. Frueh, R. S. Erwin, and M. K. Jah, "An AEGIS-FISST integrated detection and tracking approach to Space Situational Awareness," *Information Fusion, Proceedings of the 15th International Conference on*, July 2012, pp. 2065–2072.

[11] I. I. Hussein, K. J. DeMars, C. Frueh, M. K. Jah, and R. S. Erwin, "An AEGIS-FISST Algorithm for Multiple Object Tracking in Space Situational Awareness," *AIAA Guidance, Navigation, and Control Conference*, Aug. 2012.

[12] S. Gehly, B. A. Jones, and P. Axelrad, "An AEGIS-CPHD Filter to Maintain Custody of GEO Space Objects with Limited Tracking Data," *Advanced Maui Optical and Space Surveillance Technologies Conference*, Sept. 2014, p. 25.

[13] B. A. Jones, S. Gehly, and P. Axelrad, "Measurement-based Birth Model for a Space Object Cardinalized Probability Hypothesis Density Filter," *Proceedings of the 2014 AIAA/AAS Astrodynamics Specialist Conference*, Vol. 4311, Aug. 2014, p. 4311.

[14] B. A. Jones, D. S. Bryant, B.-T. Vo, and B.-N. Vo, "Challenges of Multi-Target Tracking for Space Situational Awareness," *Information Fusion, Proceedings of the 18th International Conference on*, July 2015, pp. 1278–1285.

[15] B. A. Jones and B.-N. Vo, "A Labelled Multi-Bernoulli Filter for Space Object Tracking," *2015 AAS/AIAA Spaceflight Mechanics Meeting*, Jan. 2015, pp. AAS 15–413.

[16] D. S. Bryant, E. D. Delande, S. Gehly, J. Houssineau, D. E. Clark, and B. A. Jones, "The CPHD Filter with Target Spawning," *Signal Processing, IEEE Transactions on*, Vol. pp, aug 2016, pp. 1–1.

[17] J. Houssineau, *Representation and estimation of stochastic populations*. PhD thesis, Heriot Watt University, 2015.

[18] E. D. Delande, J. Houssineau, and D. E. Clark, "Multi-object filtering with stochastic populations," *IEEE Transactions on Automatic Control*, 2016. submitted. (arXiv:1501.04671v2).

[19] E. D. Delande, C. Frueh, J. Houssineau, and D. E. Clark, "Multi-object filtering for space situational awareness," *2015 AAS/AIAA Spaceflight Mechanics Meeting*, Jan. 2015, pp. AAS 15–406.

[20] E. D. Delande, C. Frueh, J. Franco, J. Houssineau, and D. E. Clark, "A Novel Multi-Object Filtering Approach For Space Situational Awareness," *Journal of Guidance, Control, and Dynamics*, 2016. submitted.

[21] J. Houssineau and D. E. Clark, "Multi-target filtering with linearised complexity," 2016. arXiv:1404.7408v2.

[22] S. W. Shepperd, "Universal Keplerian state transition matrix," *Celestial Mechanics*, Vol. 35, No. 2, 1985, pp. 129–144.

[23] W. H. Goodyear, "Completely general closed-form solution for coordinates and partial derivative of the two-body problem," *Astronomical Journal*, Vol. 70, No. 3, 1965, pp. 189–192.

[24] R. H. Battin, *An introduction to the mathematics and methods of astrodynamics*. AIAA education series, Reston, VA: American Institute of Aeronautics and Astronautics, 1999.

[25] J. Houssineau, D. E. Clark, and P. Del Moral, "A sequential Monte Carlo approximation of the HISP filter," *2015 23rd European Signal Processing Conference (EUSIPCO)*, Aug. 2015, pp. 1251–1255.

[26] P. Del Moral, *Mean field simulation for Monte Carlo integration*. Chapman & Hall/CRC Monographs on Statistics & Applied Probability, 2013.

[27] P. Del Moral and J. Houssineau, "Particle Association Measures and Multiple Target Tracking," *Theoretical Aspects of Spatial-Temporal Modeling*, pp. 1–30, Springer, 2015.

[28] J. Franco, E. D. Delande, C. Frueh, J. Houssineau, and D. E. Clark, "A Spherical Co-ordinate Space Parameterisation for Orbit Estimation," *IEEE 2016 Aerospace Conference*, 2016.

[29] J. Franco, E. D. Delande, C. Frueh, J. Houssineau, and D. Clark, "Probabilistic Orbit Determination Using a Sensor Co-ordinate Parametrization," *Journal of Guidance, Control and Dynamics*, 2016. submitted.

[30] A. Doucet, N. d. Freitas, and N. Gordon, *Sequential Monte Carlo Methods in Practice*. Statistics for Engineering and Information Science, Springer, 2001.

[31] J. Houssineau, D. E. Clark, S. Ivekovic, C. S. Lee, and J. Franco, "A unified approach for multi-object triangulation, tracking and camera calibration," Oct. 2014. arXiv:1410.2535v1.

[32] R. E. Kalman, "A New Approach to Linear Filtering and Prediction Problems," *Journal of Basic Engineering*, Vol. 82, No. 1, 1960, pp. 32–45.

[33] K. J. DeMars and M. K. Jah, "Probabilistic Initial Orbit Determination using Radar Returns," *AAS/AIAA Astrodynamics Specialis Conference*, Aug. 2013, pp. AAS 13–704.

[34] G. Tommei, A. Milani, and A. Rossi, "Orbit determination of space debris: admissible regions," *Celestial Mechanics and Dynamical Astronomy*, Vol. 97, No. 4, 2007, pp. 289–304.

[35] D. Farnocchia, G. Tommei, A. Milani, and A. Rossi, "Innovative methods of correlation and orbit determination for space debris," *Celestial Mechanics and Dynamical Astronomy*, Vol. 107, No. 1-2, 2010, pp. 169–185.